

THE BARYONIC TULLY-FISHER RELATION OF GALAXIES WITH EXTENDED ROTATION CURVES AND THE STELLAR MASS OF ROTATING GALAXIES

STACY S. MCGAUGH

Department of Astronomy, University of Maryland and
College Park, MD 20742-2421

Draft version September 17, 2018

ABSTRACT

I investigate the Baryonic Tully-Fisher relation for a sample of galaxies with extended 21 cm rotation curves spanning the range $20 \lesssim V_f \leq 300 \text{ km s}^{-1}$. A variety of scalings of the stellar mass-to-light ratio Υ_* are considered. For each prescription for Υ_* , I give fits of the form $\mathcal{M}_d = \mathcal{A} V_f^x$. Presumably, the prescription that comes closest to the correct value will minimize the scatter in the relation. The fit with minimum scatter has $\mathcal{A} = 50 \mathcal{M}_\odot \text{ km}^{-4} \text{ s}^4$ and $x = 4$. This relation holds over five decades in mass. Galaxy color, stellar fraction, and Υ_* are correlated with each other and with \mathcal{M}_d , in the sense that more massive galaxies tend to be more evolved. There is a systematic dependence of the degree of maximality of disks on surface brightness. High surface brightness galaxies typically have $\Upsilon_* \sim \frac{3}{4}$ of the maximum disk value, while low surface brightness galaxies typically attain $\sim \frac{1}{4}$ of this amount.

Subject headings: dark matter — galaxies: kinematics and dynamics — galaxies: spiral

1. INTRODUCTION

The Tully-Fisher relation (Tully & Fisher 1977) has played an important role in establishing the extragalactic distance scale (e.g., Pierce & Tully 1988; Sakai et al. 2000). In this context, it has been treated as a simple and convenient empirical relation between luminosity and line-width. The reason why it works is also important, particularly to our understanding of galaxies as physical objects and how they formed (e.g., Eistenstein & Loeb 1996; McGaugh & de Blok 1998a; Courteau & Rix 1999; van den Bosch 2000; Navarro & Steinmetz 2000a,b). Now that the issue of the distance scale is widely considered to be settled, we can hope to place an absolute scale on galaxy mass as well as luminosity.

The physical basis of the Tully-Fisher relation is widely presumed to be a relation between a galaxy's total mass and rotation velocity (e.g., Freeman 1999). Luminosity is a proxy, being proportional to stellar mass, which in turn depends on the total mass. McGaugh et al. (2000) found that a more fundamental relationship between the baryonic mass and rotation velocity does indeed exist, provided that both stellar and gas mass are considered (Milgrom & Braun 1998).

The relation resulting from the sum of stellar and gas mass is referred to as the Baryonic Tully-Fisher (BTF) relation. The BTF has also been investigated by Bell & de Jong (2001), Verheijen (2001), Gurovich et al. (2004), and Pfenninger & Revaz (2005). These efforts find broadly similar results, in that there is such a relation. However, details of the relation differ. McGaugh et al. (2000) found a steep slope ($x \approx 4$) from a sample dominated by galaxies with *H* or *I*-band photometry and rotation velocities estimated from the line-width W_{20} . Verheijen (2001) found much the same from *K'*-band photometry and flat rotation velocities measured from resolved 21 cm cubes. Both these authors assumed a constant value of the stellar mass-to-light ratio for all galaxies. Using Verheijen's data and a grid of stellar population models to

refine the estimate of stellar mass, Bell & de Jong (2001) found a somewhat shallower slope ($x \approx 3.5$). Gurovich et al. (2004) find a break in the relation, with low mass galaxies following a steeper slope.

There is an equal variety in the physical interpretations. McGaugh et al. (2000) argue that the regularity of the BTF implies that, after the observed stars and gas are accounted for, no further comparably massive reservoirs of baryons are likely to exist in disk galaxies. Pfenninger & Revaz (2005) use the same data to argue the opposite case: the scatter is somewhat reduced if there are dark baryons weighing several times the observed gas mass. In the context of Λ CDM, one would expect still more dark baryons in order to match the universal baryon fraction (e.g., Mo & Mao 2004), though these need not be associated with the disk.

The situation at present remains confused. The purpose of this paper is to provide the best empirical BTF relation possible with the currently available data. Much depends on the value of the stellar mass. I consider the effects on the BTF of varying the stellar mass over a broad range. Mass-to-light ratios are scaled by several recipes: as a fraction of maximum disk; with respect to stellar population synthesis models; and by the Mass Discrepancy—Acceleration (MDAcc) relation (McGaugh 2004). This treats MOND (Milgrom 1983) as a purely phenomenological prescription. A grid of BTF fits are given that covers essentially any plausible choice of stellar mass-to-light ratio. The scatter of the relation varies with this choice, and an optimal choice that minimizes the scatter in the BTF relation is clear.

2. THE DATA

McGaugh et al. (2000) have already described the BTF over a large range of velocity and mass. This large dynamic range is critical to constraining the slope of the relation, and also its absolute normalization since low mass galaxies are frequently gas rich and insensitive to assumptions about Υ_* . Few other samples cover such a large dynamic range (e.g., Gurovich et al. 2004).

TABLE 1
GALAXY DATA

Galaxy	V_f (km s^{-1})	\mathcal{M}_* ($10^{10} \mathcal{M}_\odot$)	\mathcal{M}_g	μ_0	R_d (kpc)	$B - V$	Υ_{max}	Υ_{pop} ($\mathcal{M}_\odot/L_\odot$)	Υ_{acc}
UGC 2885	300	30.8	5.0	22.0	13.0	[0.47]	2.6	0.8	1.5
NGC 2841	287	32.3	1.7	21.1	4.6	0.74	7.9	2.2	3.8
NGC 5533	250	19.0	3.0	23.0	11.4	0.77	27.0	2.5	3.4
NGC 6674	242	18.0	3.9	22.5	8.3	0.57	18.0	1.1	2.6
NGC 3992	242	15.3	0.92	20.4	4.1	0.72	5.8	2.1	4.9
NGC 7331	232	13.3	1.1	21.5	4.5	0.63	5.8	1.4	2.5
NGC 3953	223	7.9	0.27	20.6	3.9	0.71	2.7	2.0	2.7
NGC 5907	214	9.7	1.1	20.7	4.0	0.78	4.7	2.6	3.9
NGC 2998	213	8.3	3.0	20.3	5.4	0.45	2.8	0.7	1.2
NGC 801	208	10.0	2.9	21.9	12.0	0.61	8.4	1.3	1.4
NGC 5371	208	11.5	1.0	21.4	7.9	0.65	3.4	1.6	1.6
NGC 5033	195	8.8	0.93	23.0	5.8	0.55	4.6	1.0	4.6
NGC 3893	188	4.20	0.56	20.3	2.3	[0.56]	2.6	1.1	2.0
NGC 4157	185	4.83	0.79	21.3	5.0	0.66	3.1	1.6	2.4
NGC 2903	185	5.5	0.31	20.5	2.0	0.55	3.6	1.0	3.6
NGC 4217	178	4.25	0.25	21.4	4.2	0.77	2.4	2.5	2.2
NGC 4013	177	4.55	0.29	21.1	3.5	0.83	4.0	3.2	3.1
NGC 3521	175	6.5	0.63	20.5	2.4	0.68	3.8	1.8	2.7
NGC 4088	173	3.30	0.79	20.9	3.1	0.51	1.7	0.9	1.1
NGC 3877	167	3.35	0.14	20.1	3.0	0.68	2.4	1.8	1.7
NGC 4100	164	4.32	0.30	20.1	2.8	0.63	2.9	1.4	2.4
NGC 3949	164	1.39	0.33	19.6	1.7	0.39	1.0	0.6	0.8
NGC 3726	162	2.62	0.62	21.6	5.5	0.45	1.8	0.7	1.0
NGC 6946	160	2.7	2.7	21.7	5.6	0.40	1.1	0.6	0.5
NGC 4051	159	3.03	0.26	21.2	4.2	0.62	1.9	1.4	1.2
NGC 3198	156	2.3	0.63	21.6	2.6	0.43	3.1	0.6	2.6
NGC 2683	155	3.5	0.05	21.1	1.2	0.65	7.0	1.6	5.8
NGC 3917	135	1.4	0.18	22.1	2.9	0.60	2.4	1.3	1.3
NGC 4085	134	1.0	0.13	20.0	1.6	0.47	1.4	0.8	1.2
NGC 2403	134	1.1	0.47	21.4	2.1	0.39	1.5	0.6	1.4
NGC 3972	134	1.0	0.12	20.6	2.1	0.55	2.1	1.0	1.5
UGC 128	131	0.57	0.91	24.2	9.2	0.60	5.0	1.3	1.1
NGC 4010	128	0.86	0.27	22.5	2.9	[0.54]	2.1	1.0	1.4
F568-V1	124	0.66	0.34	23.3	3.2	0.57	5.4	1.1	3.0
NGC 3769	122	0.80	0.53	21.1	1.7	[0.64]	1.4	1.5	1.2
NGC 6503	121	0.83	0.24	21.9	1.7	0.57	1.7	1.1	1.7
F568-3	120	0.44	0.39	23.1	4.0	0.61	4.3	1.3	1.3
NGC 4183	112	0.59	0.34	22.8	3.4	0.39	1.8	0.6	0.7
F563-V2	111	0.55	0.32	22.1	2.1	0.51	3.6	0.9	1.8
F563-1	111	0.40	0.39	23.6	4.3	0.64	9.0	1.5	3.0
NGC 1003	110	0.30	0.82	21.6	1.9	0.55	0.5	1.0	0.2
UGC 6917	110	0.54	0.20	22.9	3.4	[0.53]	3.5	1.0	1.4
UGC 6930	110	0.42	0.31	22.3	3.0	[0.59]	2.1	1.2	0.8
M 33	107	0.48	0.13	21.1	1.7	0.55	1.2	1.0	0.6
UGC 6983	107	0.57	0.29	23.0	3.6	[0.45]	4.3	0.7	1.7
NGC 247	107	0.40	0.13	23.4	2.9	0.54	3.0	1.0	1.1
NGC 7793	100	0.41	0.10	20.3	1.1	0.63	1.9	1.4	1.2
NGC 300	90	0.22	0.13	22.2	2.1	0.58	1.4	1.2	0.7
NGC 5585	90	0.12	0.25	21.9	1.4	0.46	0.8	0.7	0.5
NGC 55	86	0.10	0.13	21.5	1.6	0.54	1.0	1.0	0.2
UGC 6667	86	0.25	0.08	23.8	2.8	[0.65]	2.5	1.5	1.0
UGC 2259	86	0.22	0.05	22.3	1.3	...	3.9	...	2.1
UGC 6446	82	0.12	0.30	23.1	3.1	[0.39]	2.2	0.5	0.5
UGC 6818	73	0.04	0.10	23.5	1.9	[0.43]	0.7	0.6	0.2
NGC 1560	72	0.034	0.098	23.2	1.3	0.57	4.1	1.1	1.0
IC 2574	66	0.010	0.067	23.4	2.2	0.42	0.6	0.6	0.1
DDO 170	64	0.024	0.061	24.1	1.3	...	15.0	...	1.5
NGC 3109	62	0.005	0.068	23.1	1.6	[0.47]	1.0	0.8	0.1
DDO 154	56	0.004	0.045	23.2	0.5	0.32	2.0	0.4	0.1
DDO 168	54	0.005	0.032	23.4	0.9	0.32	0.6	0.4	0.2

One thing that stands to be improved is the accuracy of the data. The data used here are from the sample of Sanders & McGaugh (2002), as trimmed for accuracy by McGaugh (2004). The reader is referred to these papers, and references therein, for a further description of the sample. These galaxies all have extended 21 cm maps from which the flat rotation velocity V_f is measured.

The use of V_f provides a considerable improvement in accuracy over line-width measurements (Verheijen 2001). The result is a much cleaner BTF relation that is not afflicted by possible corrections to line-widths for turbulent motion. Turbulent corrections have the potential to affect the slope of the BTF by systematically adjusting the line-width inferred rotation velocities of low mass galax-

ies. In addition to resolved atomic gas measurements, all galaxies have detailed surface photometry from which stellar masses can be estimated.

The sample is identical to that in McGaugh (2004), with one exception. After re-examining the data, NGC 2915 has been replaced by UGC 6818. Though the individual data points for NGC 2915 are quite precise, this galaxy does not have a well defined V_f , the quantity of interest for the BTF. The relative distance uncertainty for NGC 2915 is also uncomfortably large (Meurer, Mackie, & Carignan 1994; Karachentsev et al. 2003). In contrast, UGC 6818 only barely missed the cut imposed in McGaugh (2004), and has more robust global measurements. Having done this exercise, I can see where further improvements could be made for individual galaxies, but these are generally very minor. These are all the galaxies that are available with an obtainably high standard of accuracy.

The data are given in Table 1. Column 1 gives the name of the galaxy. Column 2 gives V_f in km s^{-1} . These are the fit values given by Sanders & McGaugh (2002) which are the average of the outer points. As a test, I have remeasured V_f by eye for the sub-sample of Verheijen & Sancisi (2001). These agree to within a few km s^{-1} with the values given by Verheijen (2001) and with those tabulated here. V_f is easily and robustly measured, provided only that the rotation curve is extended enough. Column 3 gives the stellar mass for the mass-to-light ratio from column 10, and column 4 gives the gas mass (both in units of $10^{10} M_\odot$). Column 5 gives the central surface brightness of the disk in B mag, arcsec^{-2} , and column six the exponential disk scale length. The B -band is the only band-pass in common to all galaxies; consistent results are found in the subset with K' -band data (Sanders & Verheijen 1998; Verheijen 2001; McGaugh 2004). Column 7 gives the $B - V$ color obtained from the original source given in Sanders & McGaugh (2002) if available, or from NED¹ if not. Colors measured with CCDs are given preference; if these are not available, RC3 values are used. $B - V$ colors in square brackets are inferred from other measured colors through stellar population models. It was most often the case that $B - R$ had been measured instead of $B - V$. The colors are used to infer the mass-to-light ratio of the stellar population from said models. Several possible mass-to-light ratios are given in the last three columns: maximum disk in column 8, stellar population synthesis in column 9, and MDAcc in column 10 (McGaugh 2004).

3. METHOD

The BTF is expressed as

$$\mathcal{M}_d = \mathcal{A}V_f^x, \quad (1)$$

where \mathcal{A} is the normalization and x the slope. Note that since mass is used here rather than magnitudes, the slope m in traditional magnitude units would be $m = -2.5x$. V_f is the measured rotation velocity in the flat part of the rotation curve, and \mathcal{M}_d represents all measured² baryonic mass. It includes both stars and gas. Most of these

¹ This research has made use of the NASA/IPAC Extragalactic Database (NED) which is operated by the Jet Propulsion Laboratory, California Institute of Technology, under contract with the National Aeronautics and Space Administration.

² In McGaugh et al. (2000), this was referred to as the baryonic disk mass, hence the subscript. Both there and here the intent is to

galaxies are disk dominated, but bulge mass is included where present (see Sanders 1996). The gas mass is that measured in neutral hydrogen, corrected for helium and metals. Other gas phases are presumed to be negligible. In effect, the molecular gas mass is subsumed into the stellar mass (see discussion in McGaugh 2004). By the same token, any net internal extinction is also subsumed by Υ_* . This can not be a large effect, given the consistency between B and K' bands (Sanders & Verheijen 1998).

The baryonic mass of a galaxy is therefore

$$\mathcal{M}_d = \mathcal{M}_* + \mathcal{M}_g. \quad (2)$$

The stellar mass is given by

$$\mathcal{M}_* = \Upsilon_* L, \quad (3)$$

where Υ_* is the mass-to-light ratio of the stellar population. Fig. 1 illustrates the various Tully-Fisher relations that can be constructed from the data in Table 1: the luminosity-rotation velocity relation, $L-V_f$; this converted into stellar mass, \mathcal{M}_*-V_f ; that with gas only (no stars), \mathcal{M}_g-V_f ; and the BTF, \mathcal{M}_d-V_f .

The choice of Υ_* for each galaxy is critical. In Fig. 1, the behavior in the \mathcal{M}_*-V_f plane is markedly different from that in $L-V_f$. Use of the MDAcc mass-to-light ratio substantially reduces the scatter when mapping from L to \mathcal{M}_* . In addition, the break at $V_f \approx 90 \text{ km s}^{-1}$ noted by McGaugh et al. (2000) becomes apparent in \mathcal{M}_*-V_f , though it is not visible in $L-V_f$. Constant mass-to-light ratios were used in McGaugh et al. (2000), but the break was apparent there because of the large number of very low mass, gas dominated dwarfs. The data quality restrictions imposed here exclude those objects. Simply applying a constant Υ_* to the galaxies here would preclude the discovery of the break, since this would just be a shift in the scale of $L-V_f$. Yet a specific, well-defined method for determining Υ_* recovers the break without input about its existence.

I explore three choices for the stellar mass-to-light ratio: maximum disk, Υ_{max} ; stellar population synthesis models, Υ_{pop} ; and that from the MDAcc, Υ_{acc} . For each of these choices, I construct a grid of Υ_* scaled from each by a constant factor: Γ , \mathcal{P} , or \mathcal{Q} :

$$\Upsilon_* = \Gamma \Upsilon_{max} \quad (4)$$

$$\Upsilon_* = \mathcal{P} \Upsilon_{pop} \quad (5)$$

$$\Upsilon_* = \mathcal{Q} \Upsilon_{acc}. \quad (6)$$

This provides a prescription for Υ_* that is specified by method and scaling factor. Fig. 2 illustrates the BTF relations stemming from various choices. A few details concerning each method are worth noting here.

3.1. Scaling by Maximum Disk

Maximum disk is the highest mass-to-light ratio consistent with but not exceeding the rotation curve data. The inner shape of rotation curves are often quite consistent with the shape predicted by the observed baryons (van Albada & Sancisi 1986; Selwood 1999; Palunas & Williams 2000), leading some to argue that disks must be nearly maximal. I consider the range $0 \leq \Gamma \leq 1$.

represent all known, observed baryons, regardless of their location in the galaxy (bulge or disk).

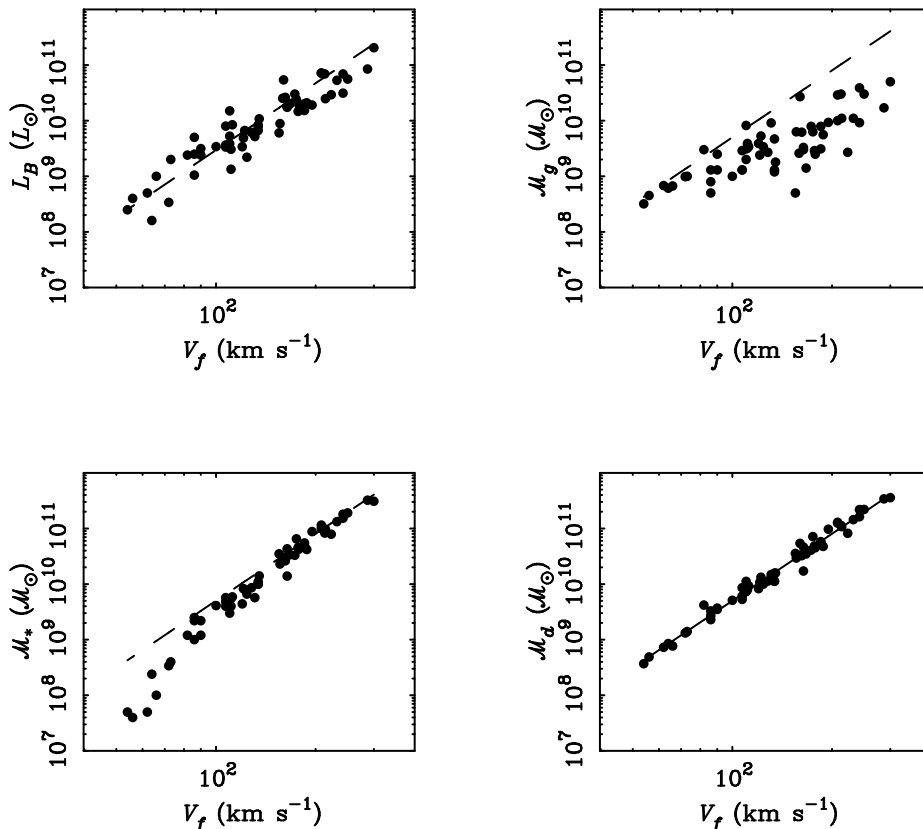


FIG. 1.— Four versions of the Tully-Fisher relation. The top left panel shows the B -band luminosity as a function of the flat rotation velocity. The top right panel plots the gas mass instead of luminosity. The bottom left panel plots stellar mass, $\mathcal{M}_* = \Upsilon_* L$ for the MDAcc mass-to-light ratios. The bottom right panel plots the Baryonic Tully-Fisher relation, with $\mathcal{M}_d = \mathcal{M}_* + \mathcal{M}_g$. The solid line is a fit to the data, $\mathcal{M}_d = 50V_f^4$. This is drawn as a dashed line in the other panels for comparison. In the top left panel, the line is drawn for the mean value $\langle \Upsilon_* \rangle = 1.7 \mathcal{M}_\odot / L_\odot$.

I adopt the maximum disk value given by the original source for the data for each galaxy (see Sanders & McGaugh 2002). Caution should be exercised in interpreting Υ_{max} . Some authors leave room for a dark halo, so that even “maximum” disk may provide only $\sim 84\%$ of the observed velocity at the peak of the disk contribution (Sackett 1997). Others leave zero room, fitting disk-only models as far out as possible (e.g., Palunas & Williams 2000). This is a fairly subtle distinction in rotation curve decompositions, but does make a noticeable difference in Υ_* . For example, the average I -band mass-to-light ratio of the Palunas & Williams (2000) sample is $\langle \Upsilon_{max} \rangle = 2.4 \mathcal{M}_\odot / L_\odot$. Since $\mathcal{M} \propto V^2$, if we scaled this down from a 100% to 84% contribution, the mean would be $\langle \Upsilon_{max} \rangle = 1.7 \mathcal{M}_\odot / L_\odot$ (see also Barnes, Sellwood, & Kosowsky 2004).

In general, there is no uniform definition of maximum disk. The data originate from a wide variety of sources, so there is no guarantee as to how maximal maximum disk is. Moreover, things can go both ways. For low surface brightness disks, very small differences in the rotation curve can lead to large changes in the inferred value of Υ_{max} (Swaters et al. 2000; McGaugh, Rubin, & de Blok 2001). For these galaxies and some of the more extreme dwarf galaxies, I have re-assessed the value of maximum disk. In spite of these caveats, the original value appears sensible for most of the galaxies in Table 1.

There are a few exceptions. For the Ursa Major data (Verheijen & Sancisi 2001), which comprises a substantial plurality of the data in Table 1, a “soft” limit was imposed on the value of Υ_{max} so that V_f of the fitted pseudo-isothermal halo did not diverge to absurdly large values (Verheijen 1997). This can easily happen for galaxies that are well described by maximum disk and for which the data are not very extended in radius. There is little clear need for a halo in such cases (Palunas & Williams 2000), so V_f is poorly constrained and tends towards large values since only the rising portion of the contribution of the dark matter is seen. Unfortunately, imposing this “soft” constraint can sometimes lead to Υ_{max} which is very sub-maximal. This is a subtle point which only became apparent because $\Upsilon_{max} < \Upsilon_{acc}$ for four of the galaxies in Table 1 (Sanders & Verheijen 1998). This is a mathematical impossibility, so I have set $\Upsilon_{max} = \Upsilon_{acc}$ in these cases.

3.2. Scaling from Stellar Population Synthesis Models

Stellar population models have advanced to the point where they give plausible estimates of the mass-to-light ratio, even for the composite stellar populations of spiral galaxies. They are not yet perfect of course, but do provide a decent choice for estimating Υ_* (Bell & de Jong 2001; Portinari et al. 2004). Here I employ the models of Bell et al. (2003) to estimate the stellar mass-to-light

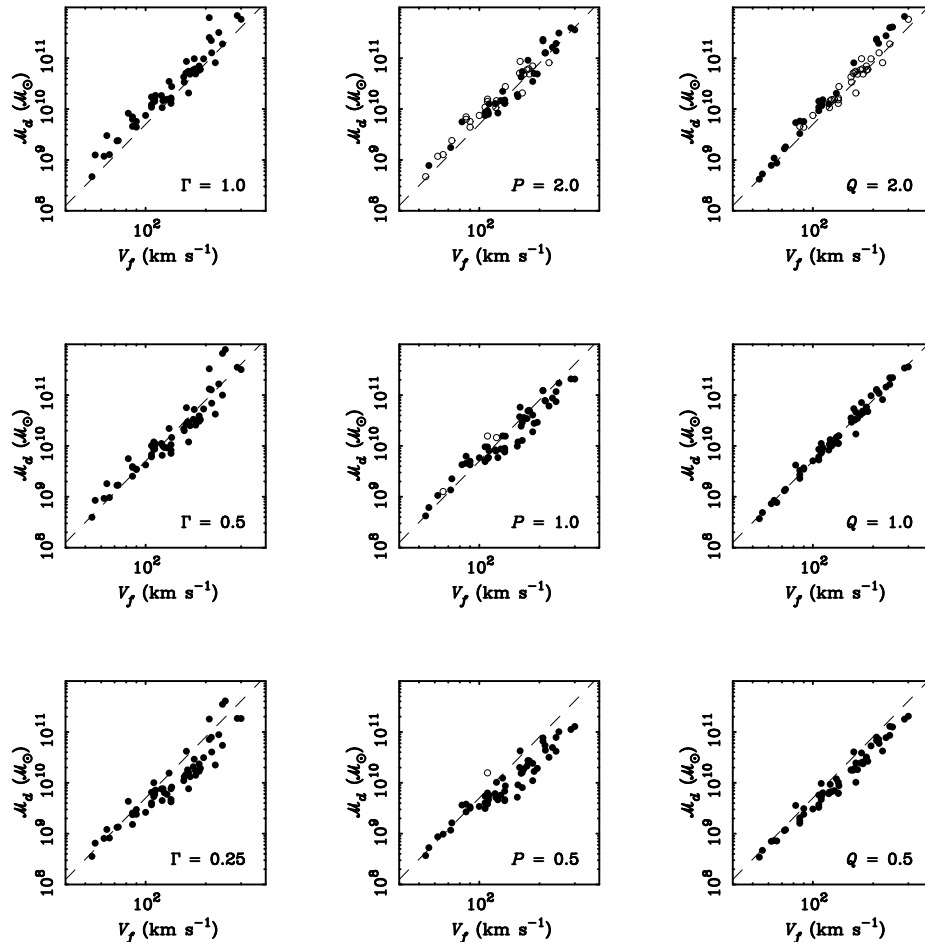


FIG. 2.— The BTF for various choices of stellar mass-to-light ratio. The left column of panels shows scalings relative to maximum disk: $\Gamma = 1, 0.5,$ and 0.25 from top to bottom. The middle column shows scalings relative to the population synthesis models of Bell et al. (2003): $P = 2, 1,$ and 0.5 from top to bottom. Similarly, the right column shows scalings relative to the mass-to-light ratio from the MDAcc: $Q = 2, 1, 0.5$ from top to bottom. (Note that $\Gamma = P = Q = 0$ are all equivalent to the gas-only panel in Figure 1.) The mass-to-light ratio is not allowed to exceed the maximum disk value. Galaxies are plotted as open symbols with their mass-to-light ratios set to the maximum disk value if the value specified by P or Q would have exceeded maximum disk. Half of the sample has reached this point by $Q = 2$. The fit to the $Q = 1$ case is shown as a dashed line in all panels for comparison.

ratio from the observed color:

$$\log \Upsilon_{pop} = 1.737(B - V) - 0.942 \quad (7)$$

(from their Table 7).

The $B - V$ color is given precedence in estimating Υ_{pop} . When $B - V$ is not available, whatever color is available is used. The most common substitute is $B - R$, which is expected to be nearly as well correlated with Υ_{\star} as $B - V$ (Bell & de Jong 2001). The same model (from Table 7 of Bell et al. 2003) is used to estimate $B - V$ (the bracketed colors in Table 1), but Υ_{pop} is based on the observed color. Credible color information could not be located for UGC 2259 and DDO 170, the only pieces missing from Table 1.

3.3. Scaling from the Mass-Discrepancy—Acceleration Relation

McGaugh (2004) used the detailed shapes of the rotation curves of the galaxies in Table 1 to show that there is an empirical relation between acceleration and the amplitude of the mass discrepancy (essentially the ratio of dark to baryonic mass). This relation holds at

every point along a resolved rotation curve for any non-zero choice of mass-to-light ratio. The scatter about this relation depends on this choice; Υ_{acc} is determined by minimizing the scatter with respect to the mean *local* relation. It is interesting to see here how this Υ_{\star} estimator fares with the *global* BTF.

The MDAcc is a purely empirical relation. It is mathematically equivalent to MOND: the Υ_{acc} are the same as the MOND best fit values (Begeman, Broeils, & Sanders 1991; Sanders 1996; Sanders & Verheijen 1998; de Blok & McGaugh 1998). Here we must make the distinction between MOND as a fundamental theory (with its associated difficulties), and as a successful recipe for fitting rotation curves. Only the latter is required. Indeed, the MDAcc is the local analog of the BTF, and had MOND never been invented, we would perhaps already have recognized the MDAcc purely as an empirical relation (Sancisi 2003). Just as the Tully-Fisher relation can be used empirically to estimate distances without understanding its physical basis, so too can the MDAcc be utilized to estimate stellar mass-to-light ratios without prejudice concerning its theoretical basis.

4. RESULTS

Equations (4-6) are used to estimate the stellar mass for the various scalings. For each scaling, a grid of 10 choices of the scaling constant are made: $\Gamma = 0.1$ to 1.0 in steps of 0.1 relative to maximum disk, and for \mathcal{P} and \mathcal{Q} values ranging from 0.2 to 2.0 in steps of 0.2. The maximum disk scaling obviously can not exceed unity, while for the other scalings there is no reason not to consider values larger than one. For example, $\mathcal{P} > 1$ would simply imply an IMF heavier than assumed in the nominal population model which has been adopted. However, these values should not exceed maximum disk, and are not allowed to do so. If the choice of \mathcal{P} or \mathcal{Q} exceeds the maximum disk value for a particular galaxy, the maximum disk value is used instead. Half of the sample has saturated at maximum by $\mathcal{Q} = 2$, so larger values are not considered.

The BTF (logarithm of equation 1) is fit³ to the data in Table 1 for each set of choices for Υ_* . Every galaxy carries equal weight in the fits. Since the data have been selected to be of high quality, the residual uncertainties are likely to be dominated by systematic effects (such as the precise distance to each galaxy) rather than factors internal to the data, though these obviously matter as well. In any case, the choice of mass-to-light ratio completely dominates the results.

The results of fitting the BTF are given in Table 2. The intercept $\log \mathcal{A}$ and slope x are recorded, together with the formal uncertainties in each ($\sigma_{\mathcal{A}}$ and σ_x). Also given is the scatter of the data about each relation, $\sigma_{\mathcal{M}}$. For reference, the input data, in the form of the normal luminosity-based Tully-Fisher relation is given. It has a scatter $\sigma_L = 0.24$, which is equivalent to 0.6 mag. (base ten logarithms are used throughout). Note also that the limit $\Gamma = \mathcal{P} = \mathcal{Q} = 0$ is equivalent to the gas-only relation, so is given only once.

The results summarized in Table 2 are illustrated in Figs. 3 and 4. As the assumed mass-to-light ratio increases, the slope x gradually increases while the zero point \mathcal{A} decreases to compensate. The lowest mass galaxies in Table 1 are dominated by gaseous rather than stellar mass, so the BTF tends to pivot about them. This can be seen by eye in Fig. 2, where the low end of the relation hardly budes while the more massive, star dominated galaxies move up and down with Υ_* . These low mass, gas-rich galaxies provide a critical anchor point for the absolute calibration of the BTF since their location in this diagram is insensitive to the choice of Υ_* .

The scatter $\sigma_{\mathcal{M}}$ about each fit is shown in Fig. 4. The maximum disk scaling has scatter comparable to the scatter in the input luminosities. The use of color information with population synthesis models provides a small increment of improvement in the scatter, as it should if the models succeed in improving the estimate of Υ_* over a constant value for all objects. As stellar mass is rendered unimportant for very small Γ and \mathcal{P} the scatter starts to increase. The limit of zero stellar mass, with gas only, obviously makes for an inadequate BTF, as one would expect.

4.1. *The Optimal BTF*

³ These are ‘direct’ fits. The scatter is small enough that forward and reverse fits are not distinguishable except in the limit $\Upsilon_* \rightarrow 0$.

TABLE 2
BTF STATISTICS

	$\log \mathcal{A}$	$\sigma_{\mathcal{A}}$	x	σ_x	$\sigma_{\mathcal{M}}$
L_B	Luminosity (Normal TF)				
1.0	2.52	0.37	3.48	0.17	0.239
\mathcal{M}_g	Gas Only				
0.0	4.67	0.48	2.28	0.48	0.313
Γ	Maximum Disk Scaling				
0.1	3.24	0.37	3.09	0.37	0.244
0.2	2.76	0.35	3.38	0.35	0.230
0.3	2.50	0.35	3.55	0.35	0.224
0.4	2.34	0.34	3.67	0.34	0.222
0.5	2.23	0.34	3.75	0.34	0.220
0.6	2.15	0.34	3.81	0.34	0.220
0.7	2.09	0.34	3.87	0.34	0.220
0.8	2.05	0.34	3.91	0.34	0.220
0.9	2.01	0.34	3.94	0.34	0.220
1.0	1.98	0.34	3.97	0.34	0.221
\mathcal{P}	Population Synthesis Scaling				
0.2	3.81	0.33	2.81	0.15	0.204
0.4	3.44	0.30	3.04	0.14	0.186
0.6	3.23	0.29	3.19	0.14	0.183
0.8	3.08	0.29	3.29	0.13	0.183
1.0	2.98	0.29	3.37	0.13	0.186
1.2	2.87	0.28	3.44	0.13	0.188
1.4	2.75	0.27	3.52	0.13	0.191
1.6	2.65	0.27	3.58	0.13	0.194
1.8	2.54	0.26	3.64	0.12	0.197
2.0	2.46	0.26	3.69	0.12	0.200
\mathcal{Q}	MDAcc Scaling				
0.2	3.05	0.25	3.18	0.25	0.165
0.4	2.46	0.20	3.53	0.20	0.129
0.6	2.11	0.17	3.74	0.17	0.112
0.8	1.87	0.16	3.89	0.16	0.103
1.0	1.70	0.15	4.00	0.15	0.098
1.2	1.60	0.15	4.07	0.15	0.100
1.4	1.58	0.16	4.10	0.16	0.107
1.6	1.60	0.18	4.10	0.18	0.118
1.8	1.61	0.20	4.10	0.20	0.129
2.0	1.64	0.22	4.10	0.22	0.140

Irrespective of the physics underlying the BTF, we expect that the prescription for Υ_* that comes closest to the correct value will minimize the scatter about it. There may be some intrinsic scatter, but if we can get Υ_* right, there should be no scatter left due to it. The Υ_{acc} prescription gives less scatter than either Υ_{max} or Υ_{pop} . There is clear variation in the scatter with \mathcal{Q} , with a well defined minimum at $\mathcal{Q} = 1$. The same mass-to-light ratio chosen to minimize the residuals from the local MDAcc also minimizes the scatter in the global BTF. This was already apparent in Fig. 6 of McGaugh (2004), and is quantitatively confirmed here. It is rare in extragalactic astronomy that we find a correlation as strong as the BTF ($\mathcal{R} = 0.99$ for $\mathcal{Q} = 1$). Indeed, the BTF is so sharply defined that it has a kurtosis of 1.5.

It is difficult to avoid the conclusion that the choice $\mathcal{Q} = 1$ does effectively give the correct Υ_* . This provides an absolute calibration of the BTF:

$$\mathcal{M}_d = 50V_f^4 \quad (8)$$

with \mathcal{M}_d in \mathcal{M}_{\odot} and V_f in kms^{-1} . Indeed, the scatter in this BTF relation is so small that it could be used to estimate Υ_* with nearly as great accuracy as the full

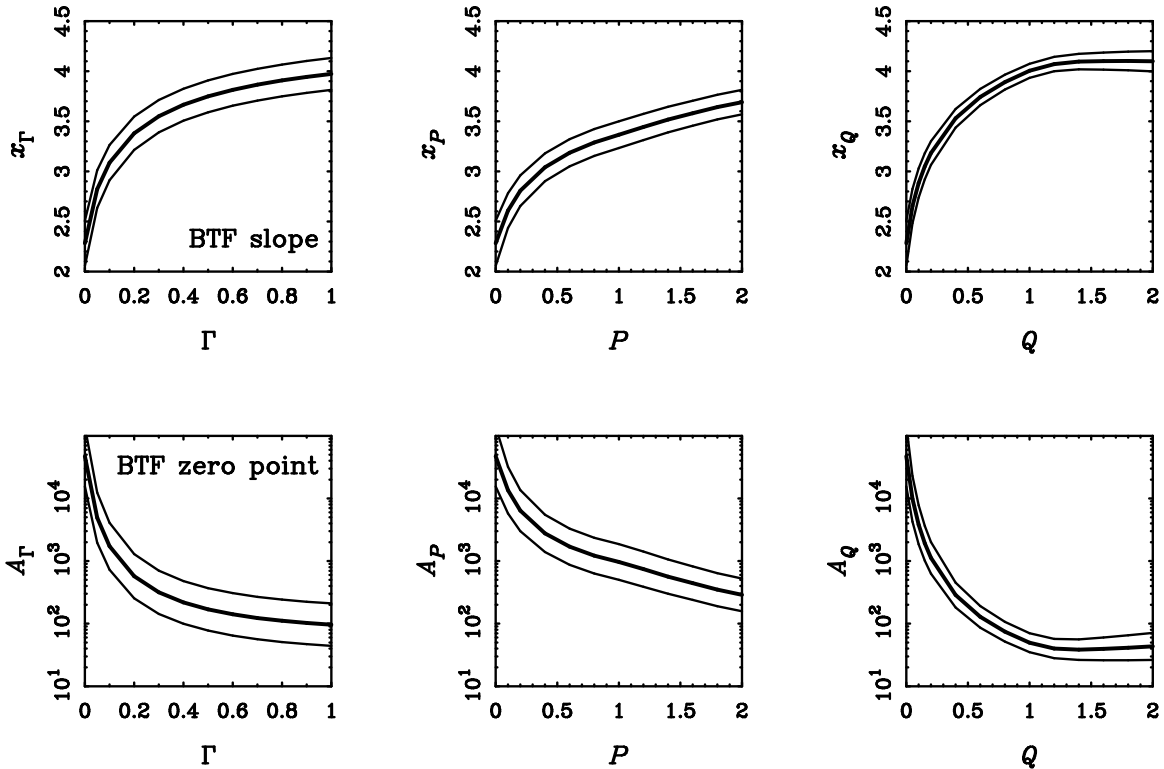


FIG. 3.— The slope (top panels) and zero point (bottom panels) of the BTf for various scalings of the stellar mass-to-light ratio: as a fraction of maximum disk (left panels), relative to population synthesis models (middle panels), and relative to the MDAcc mass-to-light ratios (right panels). For each choice of Υ_* , the data have been fit as a straight line to the logarithm of $\mathcal{M}_d = \mathcal{A}V_f^x$ (Table 2). The thin lines show the formal uncertainties on the parameters $\log \mathcal{A}$ and x of the fit. For all scalings, the slope of the mass—circular velocity BTf only becomes as shallow as $x = 3$ for implausibly small mass-to-light ratios.

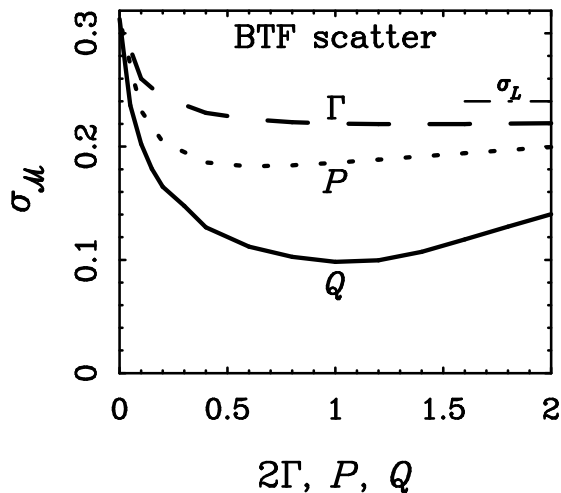


FIG. 4.— The scatter $\sigma_{\mathcal{M}}$ in the BTf for the various scalings of mass-to-light ratio. Dashed line: maximum disk (plotted against 2Γ to fill the same range as the other choices). Dotted line: population synthesis. Solid line: mass-to-light ratios from the MDAcc. The latter show a clear minimum at $Q = 1$. The other scalings have no clearly defined minima, and larger scatter for all choices of Γ or P . The ordinary Tully-Fisher relation of the input data has a scatter of $\sigma_L = 0.24$ (dash-dot line).

MDAcc, but with considerably less information. To apply the latter, we require a well resolved rotation curve and HI surface density map, and detailed surface photometry. The BTf requires only global quantities: L ,

\mathcal{M}_g from a single dish 21 cm observation, and an estimate of V_f (preferably from a rotation curve which is sufficiently resolved to perceive the flat part, though $\frac{1}{2}W_{50}$ would be an adequate substitute, with some penalty in accuracy.)

This BTf is consistent with the relation first reported by McGaugh et al. (2000). The slope is identical, but the normalization is somewhat larger. This change is not particularly significant (1σ). It is largely due to the improvement in data quality and the use of V_f rather than $\frac{1}{2}W_{20}$. The line-width W_{20} is systematically larger than $2V_f$, which is more closely approximated by W_{50} (Broeils 1992; Verheijen 1997). Thus we should expect some increase in \mathcal{A} simply from the change of circular velocity measures.

Indeed, it is reassuring that the relation found here is so closely consistent with the previous version. McGaugh et al. (2000) chose Υ_* by a different method, taking a constant value for all galaxies motivated by population models. More importantly, the data are largely independent: the BTf of McGaugh et al. (2000) included 110 galaxies from Bothun et al. (1985), 14 from Matthews, van Driel, & Gallagher (1998), and 65 from Eder & Schombert (2000) that are completely distinct from and independent of the data in Table 1. The agreement of such diverse and independent data sets provides strong confirmation of the basic empirical result.

4.2. Correlations Among Evolutionary Parameters

TABLE 3
CORRELATION COEFFICIENTS

	\mathcal{M}_d	f_*	Υ_*	$B - V$
V_f	0.99	0.78	0.77	0.53
\mathcal{M}_d	...	0.76	0.76	0.53
f_*	0.84	0.54
Υ_*	0.64

The BTF is by far the strongest correlation present in the data, but it is not the only one. There are a few others worth noting. Some of these are shown in Fig. 5. Many others are not shown to avoid redundancy: anything that is correlated with disk mass is also correlated with V_f through the BTF. Correlation coefficients for the quantities appearing in Fig. 5 are given in Table 3.

One interesting quantity that can be constructed from the data in Table 1 is the fraction of the total observed baryonic mass in the form of stars: $f_* = \mathcal{M}_*/\mathcal{M}_d$. The variation of f_* with disk mass basically shows the turn-away of the stellar mass TF from the BTF as one goes from star to gas domination. There is lots of scatter in the $f_*\text{-}\mathcal{M}_d$ diagram which is not reflected in the BTF. This reiterates that what matters is mass, not the form it is in.

Together with the mass-to-light ratio and color, f_* is an indicator of the evolutionary state of a galaxy (McGaugh & de Blok 1997, 1998a; Schombert, McGaugh, & Eder 2001). As evolution proceeds and a galaxy converts its initial gas into stars, the stellar fraction increases. As old stars accumulate, the mean color reddens, and the mass-to-light ratio increases. One therefore expects these quantities to be related.

The evolutionary quantities f_* , Υ_* , and color do indeed correlate as expected. Not only does the mass-to-light ratio increase as the stellar population reddens, so too does Υ_* climb as f_* increases. Indeed, the $\Upsilon_*\text{-}f_*$ correlation is the next strongest in Table 3 after the BTF.

In this sample, the evolutionary quantities are correlated with baryonic mass. They are also correlated with V_f , as shown previously by Sanders (1996). This must follow, given the BTF. Indeed, figures constructed with V_f instead of \mathcal{M}_d look so similar that they are difficult to distinguish.

One curious feature of the correlations with disk mass is that all of the evolutionary indicators suggest that more massive disks are typically more evolved. This is opposite what one might naively expect from a hierarchical galaxy formation picture. In such a scenario, small galaxies form first so should have evolved the most. That the opposite is true seems more consistent with monolithic or even top-down galaxy formation. Similar results have been found recently at high redshift (e.g., Juneau et al. 2005; Treu et al. 2005), where the tendency for massive galaxies to be the most evolved is called “downsizing.” If galaxies do form hierarchically, the observed trend suggests that the mechanisms which regulate a galaxy’s post-formation evolution dominate over the formation epoch in determining its present evolutionary status. This would appear to be a continuous function of mass, given the continuity in Fig. 5. It does not appear to

be as simple as a single epoch of reionization suppressing galaxy formation at a characteristic mass scale.

One word of caution is that while these data span a broad range of galaxy properties, they do not constitute a complete volume limited sample. The details of these correlations may well change as other data are added. Nevertheless, it seems unlikely that the trend apparent in this figure could be reversed: massive galaxies still in the early stages of evolution seem to be very rare.

It is extremely difficult to obtain a sample extending to very low mass which is complete in any meaningful sense. Since an HI map is a prerequisite for membership in this sample, it seems likely that there are some low mass, high f_* galaxies which are not represented here. So while there are some clear correlations with disk mass *in this sample*, there is no guarantee that precisely these correlations will hold for all galaxies. There is more hope that correlations between the evolutionary parameters f_* , Υ_* , and $B - V$ will hold, if only because they make so much sense.

These cautions do not apply to the BTF. There is no hint of deviation from it: the residuals are small and uncorrelated with any measured parameter. There is no reason to suspect that any rotating galaxy deviates from the BTF — even those that should deviate do not (McGaugh & de Blok 1998a; Verheijen 2001). The BTF appears to be a fundamental relation.

4.3. Consistency with Stellar Population Models

The remarkable consistency of the MDAcc mass-to-light ratios with stellar population synthesis models has been noted previously (Sanders 1996; McGaugh & de Blok 1998b; Sanders & McGaugh 2002; McGaugh 2004). I have added more color information to the data in Table 1 than has previously been available, and this point remains true. Indeed, there are now enough data that we can perform a fit in the same manner as done for population synthesis models. Following the format of Bell & de Jong (2001), the data are fit to a relation of the form

$$\log \Upsilon_* = a - b(B - V). \quad (9)$$

Portinari et al. (2004) note that while their B -band model Υ_* are linearly correlated for $B - V > 0.55$, they show a break at this point. Υ_* turns down to lower values for bluer colors than predicted by extrapolation of the line fit to redder colors. I therefore consider two fits to the data: one covering data of all colors, and the other restricted to $B - V > 0.55$.

The relations from the stellar population synthesis models of Bell et al. (2003) and Portinari et al. (2004) are compared with the fits to the data in Table 4. The relation of Bell et al. (2003) is that used to estimate Υ_{pop} (equation 7). Note the close agreement between the two models: these are virtually indistinguishable in Fig. 5. The zero points a of the models are dominated by the choice of IMF, which is fortuitously close (Kroupa & Weidner 2003).

There is close agreement between the parameters a and b fit to the data and those predicted by the models. The MDAcc mass-to-light ratios, determined by dynamical methods completely independent of the population models, show precisely the same trends. A slight offset in normalization is apparent, but its formal significance is

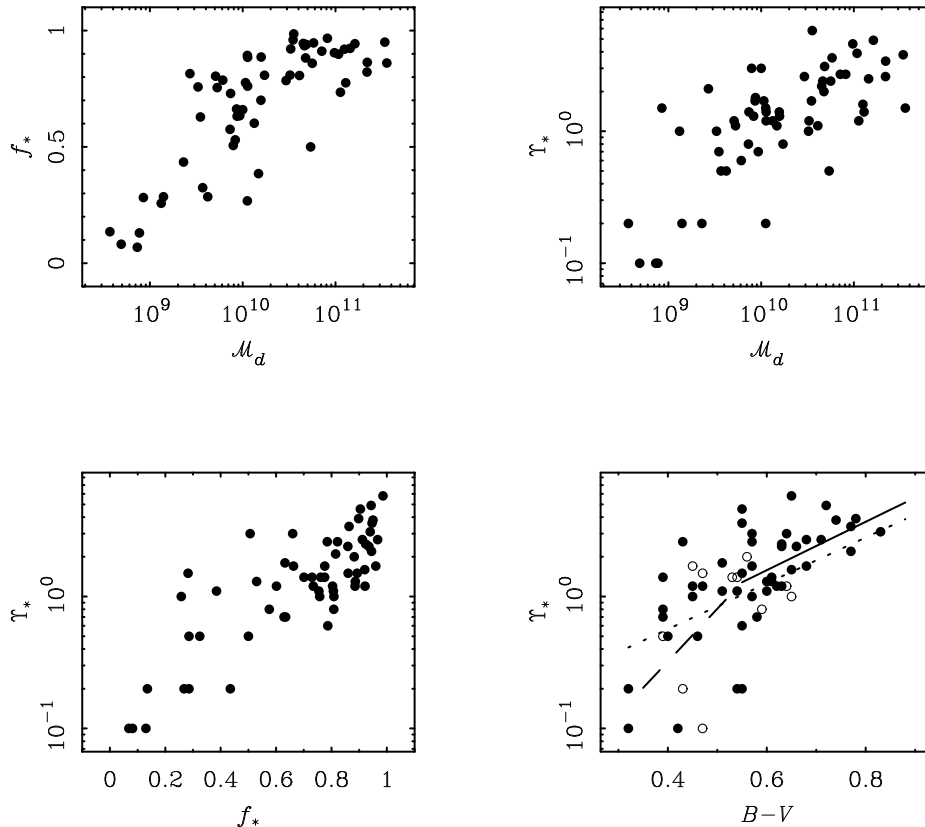


FIG. 5.— Some of the stronger correlations in the current sample beyond the BTF. The stellar mass fraction f_* is correlated with disk mass and Υ_* (left panels). The mass-to-light ratio is also correlated with disk mass and color (right panels). In the Υ_* — $(B - V)$ diagram at bottom right, a fit to the data is shown as a solid line. The fit shown is to data with $B - V > 0.55$, where one expects a break in the Υ_* — $(B - V)$ relation (Portinari et al. 2004). The dashed line has the slope expected for $B - V < 0.55$ in their models, with normalization chosen to match the fit to the data at $B - V = 0.55$. For comparison, the dotted line shows the model mass-to-light ratio—color relation of Bell et al. (2003) which has been used to define $\mathcal{P} = 1$.

TABLE 4
MASS-TO-LIGHT RATIO—COLOR RELATIONS

Source	a	b	Note
Bell et al.	-0.942	1.737	Scaled Salpeter IMF
Portinari et al.	-0.925	1.69	Kroupa IMF
Fit to the Data	-0.90	1.83	$B - V > 0.55$
Fit to the Data	-1.22	2.31	All colors

NOTE. — Relations of the form $\log \Upsilon_* = a + b(B - V)$.

low. It is tempting to interpret this offset as the molecular gas which has been subsumed into Υ_{acc} . If the mass of gas in the molecular phase is typically 10% to 20% of that in stars, the offset between models and data would be reconciled.

The break at $B - V \approx 0.55$ in the models of Portinari et al. (2004) is apparent in the data. Fig. 5 shows (as the dashed line) the model slope for bluer colors (from their Fig. 28), normalized to match the fit to the data at the break point. This is entirely consistent with the downward trend in the data.

The scatter in Υ_* is also as expected, being larger in B than in K' (Sanders & McGaugh 2002; McGaugh 2004). This is true also above and below the break point at

$B - V = 0.55$. Below this point, one expects a tremendous amount of scatter from the rapid evolution of young populations. Here the scatter is enormous: $\sigma_{\Upsilon_*} = 0.52$. Above this color, one expects variation in Υ_* to settle down, as the effects of individual star formation events are moderated by the accumulation of mass from previous generations. For these redder colors, the scatter is $\sigma_{\Upsilon_*} = 0.20$.

In sum, the $\mathcal{Q} = 1$ mass-to-light ratios are optimal not only in terms of minimizing the scatter in the BTF and the MDAcc (from which they come), but also in terms of our expectations for stellar populations. Indeed, it is hard to imagine better agreement with independent population models to which no fit has been made. Moreover, the scatter in the dynamical relations is so small for these high quality data that Υ_* estimated from the BTF itself (equation 7) are nearly indistinguishable from Υ_{acc} from the MDAcc. Either empirical method can be employed with unprecedented precision.

4.4. Test by Extrapolation

The value of the slope x of the BTF is somewhat controversial, being of considerable physical importance. The nominal expectation of CDM is that $x = 3$ (Navarro & Steinmetz 2000a,b), and Courteau et al. (2003) argue that this is consistent with their I -band data. The I -band is a good but not perfect indicator of mass, and

the HST calibrated distances of Sakai et al. (2000) give an I -band slope of 4. This emphasizes the need for a good estimate of \mathcal{M}_d and not just L .

McGaugh et al. (2000) found $x = 4$ from data and Υ_* estimates independent of those used here. The key aspect of that study was the large number of very gas rich, low rotation velocity galaxies which tied down the low mass end of the BTF. Verheijen (2001) obtained the same result. Bell & de Jong (2001) generated stellar population models in an attempt to improve the estimate of Υ_* . Applied to the data of Verheijen, they found a BTF with $x = 3.5$. I have, in effect, repeated this analysis with more data and updated models, and find very much the same result: for $\mathcal{P} = 1$, $x = 3.4$ (Table 2).

It is interesting that while the models and data are in good agreement (§4.2), use of Υ_{pop} gives somewhat shallower x than Υ_{acc} or Υ_{max} (Fig. 3). This is attributable in part to the slight difference in normalization (a in Table 4). This can not be the entire reason for the difference, as increasing \mathcal{P} to 2 only increases x to 3.7. The shortcoming of Υ_{pop} estimated from a single color is that galaxies become beads on a string in the Υ_* -($B - V$) diagram: all the data collapse to fall on the dotted line in Fig 5. The inability to estimate deviations from the mean relation and thereby include a realistic estimate of the scatter seems to result in a bias⁴ in the determination of the slope. Relative to the population predicted Υ_{pop} , Υ_{acc} is skewed to high values for red colors and to low values for blue colors. One expects such a skew relative to a single straight line fit (Portinari et al. 2004); it causes a systematic difference in the slope in spite of the close agreement seen in Fig. 5 and Table 4.

The critical issue for constraining the slope is the dynamic range of the data. As a further test of the slope of the BTF, I have sought out galaxies that extend the relation to lower rotation velocities. The slowest rotator in Table 1 has $V_f = 54 \text{ km s}^{-1}$. I have searched the literature for galaxies with slower rotation velocities that are of adequate quality to make a useful comparison. There are many slow rotators already in the sample of McGaugh et al. (2000), but there the rotation velocity estimate was based on a line-width (Eder & Schombert 2000). Here I require that there be a resolved measurement adequate for estimating V_f .

Table 5 contains the objects found that met these criteria. Many of these are due to the recent excellent work of Begum & Changalar (2003, 2004a,b) which extends down to objects approaching the globular cluster mass scale. In Table 5 I give the data necessary for the BTF from the data given in each reference cited there. I have estimated V_f myself from the published data. In addition to the best estimate, I give a generous range of uncertainty. In many of these cases, there is a substantial correction for asymptotic drift. The lower limit of V_f takes the lower end of the published errors ignoring the asymptotic drift correction. The upper limit takes the upper end of the experimental errors and includes the correction. This procedure results in a very broad error estimate: the uncertainties listed in Table 5 are much

⁴ One could, perhaps, do better with more colors. The incorporation of such information had an analogous effect on the slope of the K' -band Υ_* -color relation, which became flatter between Bell & de Jong (2001) and Bell et al. (2003).

TABLE 5
EXTREME DWARF GALAXY DATA

Galaxy	V_f (km s^{-1})	\mathcal{M}_* ($10^6 \mathcal{M}_\odot$)	\mathcal{M}_g	Ref.
ESO215-G?009	51 $^{+8}_{-9}$	23	714	1
UGC 11583 ^a	48 $^{+3}_{-4}$	119	36	2,3
NGC 3741	44 $^{+4}_{-2}$	25	224	4
WLM	38 $^{+5}_{-5}$	31	65	5
KK98 251	36 $^{+8}_{-4}$	12	98	3
GR 8	25 $^{+5}_{-4}$	5	14	6
Cam B	20 $^{+10}_{-13}$	3.5	6.6	7
DDO 210	17 $^{+3}_{-5}$	0.9	3.6	8

REFERENCES. — 1. Warren, Jerjen, & Koribalski (2004). 2. McGaugh, Rubin, & de Blok (2001). 3. Begum & Chengalur (2004a). 4. Begum, Chengalur, & Karachentsev (2005). 5. Jackson et al. (2004). 6. Begum & Chengalur (2003). 7. Begum, Chengalur, & Hopp (2003). 8. Begum, & Chengalur (2004b).

^aUGC 11583 = KK98 250.

larger than 1σ .

For the stellar and gas mass, I take the value given by the original authors. \mathcal{M}_* has often been estimated using the models of Bell & de Jong (2001), so these correspond roughly to $\mathcal{P} = 1$ estimates. Rather than an uncertainty, I consider the full range of possible stellar masses, from zero to maximum disk. These are the vertical lines in Fig. 6.

The extrapolation of the BTF fit to the data in Table 1 does an excellent job of predicting the data for these lower mass galaxies. The objects in Table 5 follow the slope $x = 4$ down to unprecedented low velocity. The BTF remains valid over five decades in mass.

Fig. 6 also illustrates why the slope has been difficult to constrain. The lower limit of other studies ($\sim 10^9 \mathcal{M}_\odot$, $V_f \approx 70 \text{ km s}^{-1}$: e.g., Bell & de Jong 2001; Courteau et al. 2003) is shown in the left hand panel. The data considered there extend over only a small fraction of the range studied here (down to $5 \times 10^6 \mathcal{M}_\odot$ with the extreme dwarfs in Table 5). This lack of dynamic range probably dominates all other factors (such as the mass determination method or the velocity estimator used) in constraining the slope. Indeed, if we were to truncate the data in Table 1 at the same level, we would fail to perceive the break-point in the stellar mass Tully-Fisher relation. Such a sample would be dominated by star-dominated galaxies, and fail to provide the constraint on Υ_* which follows when gas-dominated objects are included.

The steep slope of the BTF should come as no surprise, as it is completely consistent with the results of McGaugh et al. (2000). That study made use many low mass galaxies, 19 of which have $\frac{1}{2}W_{20} < 70 \text{ km s}^{-1}$. Those objects are completely independent of the galaxies discussed here. The new, more accurate data in Table 5 simply return the same result with less scatter. Other workers investigating low mass galaxies have also inferred the need for a steep slope (e.g., Gurovich et al. 2004; Pizagno et al. 2004).

Formally, a slope as shallow as $x = 3$ deviates from the

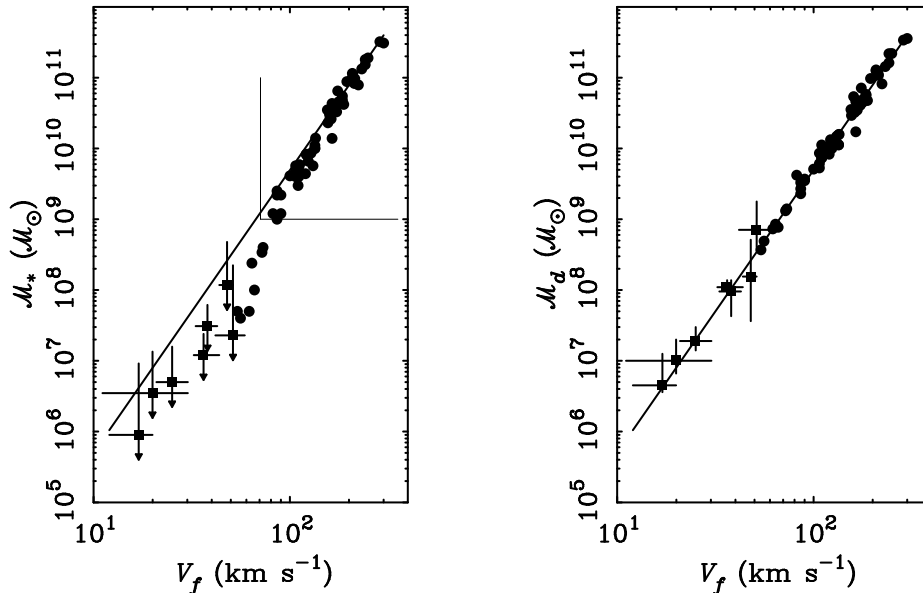


FIG. 6.— The stellar mass (left) and baryonic (right) Tully-Fisher relations, including the data for the extreme dwarf galaxies listed in Table 5. The horizontal lines through these objects are the maximum plausible range for V_f : these are much larger than 1σ error bars. The vertical lines show the full range of possible stellar masses, from zero to maximum disk. The extrapolation of the BTF fit to the more massive galaxies from Table 1 is in good agreement with these extreme dwarfs. The importance of this check is illustrated by the thin lines inset in the left panel. These show the limits of samples that suggest shallower slopes (e.g., Bell & de Jong 2001; Courteau et al. 2003).

optimal BTF by 7σ . This can be made less by changing Υ_* , but only at the price of degrading the correlation and the many consistency checks on Υ_* . In order to recover a slope as shallow as $x = 3$, one requires $\mathcal{P} = 0.36$ or $\Gamma < 0.1$ (Table 2). Such absurdly sub-maximal disks would fall considerably short of the mass which is directly observed in stars locally.

Consideration of the extreme dwarfs renders it even more difficult to reconcile a shallow slope with the data. While it is possible, at least in principle, to move massive galaxies down in mass by reducing their mass-to-light ratios in order to accommodate a shallow slope, it is not possible to move the extreme dwarfs very far up. Even taking maximum disk in those cases makes little difference to the slope, and causes the curious situation that the IMF in these low mass galaxies must be systematically heavier than that in giant galaxies. It is thus very difficult to reconcile a shallow ($x = 3$) slope for the BTF with the data.

4.5. The Maximality of Disks

One application of the result here is to quantify the degree to which galaxy disks are maximal. There is considerable debate as to whether high surface brightness disks are maximal (e.g., Sellwood 1999; Courteau & Rix 1999). There would seem little doubt that low surface brightness disks are dark matter dominated (de Blok & McGaugh 1997, 2001), but an argument for maximal disks can be made even in these objects (Fuchs 2003). It is therefore of considerable interest to investigate how maximal disks are, and how disk maximality varies with disk properties.

For the MDAcc mass-to-light ratios favored here, the fraction of maximum disk in each case is

$$\Gamma_* = \frac{\Upsilon_{acc}}{\Upsilon_{max}}. \quad (10)$$

This is plotted against disk mass and surface density

in Fig. 7. There is only a weak correlation of Γ_* with disk mass ($\mathcal{R} = 0.45$) which depends heavily on rather few points at low mass (cf. Persic & Salucci 1988). Dynamical arguments stemming from the adherence of low surface brightness galaxies to the Tully-Fisher relation (Zwaan et al. 1995; Sprayberry et al. 1995; Hoffman et al. 1996) suggest that disk maximality Γ_* should correlate with surface brightness (Tully & Verheijen 1997; McGaugh & de Blok 1998a; Zavala et al. 2003). We can improve on this by using the mass-to-light ratios Υ_{acc} to convert the observed central surface brightness into the central surface mass density of stars:

$$\log \Sigma_0 = \log \Upsilon_{acc} + 0.4(27.05 - \mu_0). \quad (11)$$

As anticipated, there is a good correlation between Γ_* and Σ_0 ($\mathcal{R} = 0.74$). A fit to the data in Fig. 7 gives

$$\log \Gamma_* = -0.98 + 0.3 \log \Sigma_0. \quad (12)$$

In terms of the more directly observable central surface brightness, this translates to $\log \Gamma_* = 3.13 - 0.16\mu_0$. There is considerably greater scatter about this latter relation.

Irrespective of how we frame the relation, or what mass-to-light ratio prescription we prefer, it seems inevitable that the disk contribution must decline systematically as surface density declines. Low surface brightness disks are inevitably dark matter dominated. In contrast, high surface density disks contribute a non-negligible fraction of the total mass at small radii for plausible Υ_* . Remarkably, this leaves no residual signature in the Tully-Fisher relation (McGaugh & de Blok 1998a; Courteau & Rix 1999) in spite of the generally modest radius at which rotation curves achieve V_f .

Statistics of these data, divided into quartiles by Σ_0 , are given in Table 6. The typical $\Gamma_* = 0.78$ in the highest surface density quartile. Γ_* can not exceed unity, and is projected to saturate at $\mu_0 \approx 19.5 \text{ mag. arcsec}^{-2}$.

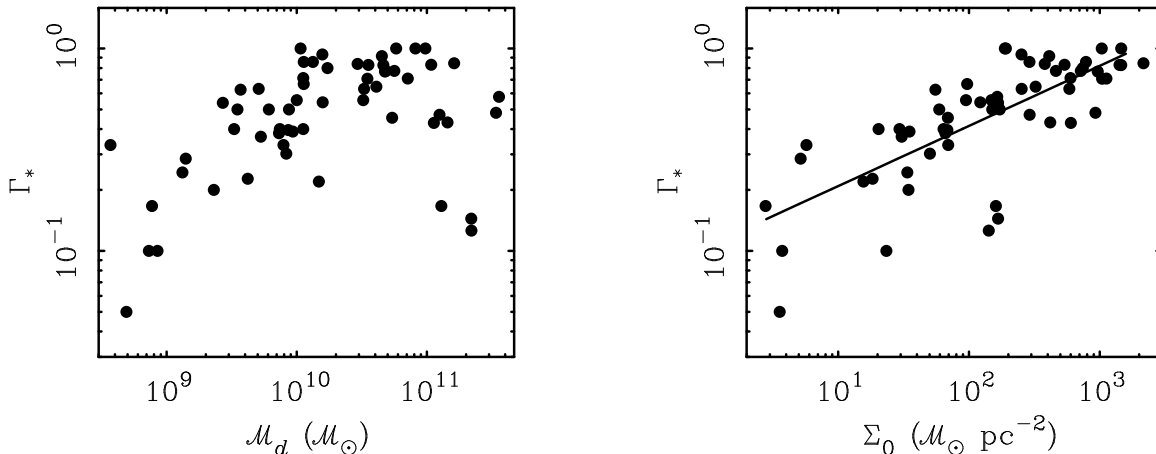


FIG. 7.— The maximality of disks (Γ_* for $\mathcal{Q} = 1$) as a function of disk mass (left) and the central stellar surface mass density (right). While the correlation with mass is poor, there is a clear correlation of maximality with disk surface density. High surface density disks tend to be nearly maximal, while lower surface density disks are systematically sub-maximal. The line is a fit to the data (equation 12).

TABLE 6
MAXIMALITY OF DISKS

Quartile	N	$\langle \mu_0^B \rangle$ (mag. arcsec $^{-2}$)	$\langle \Sigma_0 \rangle$ ($\mathcal{M}_\odot \text{ pc}^{-2}$)	$\langle \Gamma_* \rangle$
1	15	23.31	21	0.25
2	15	22.31	99	0.48
3	15	21.52	295	0.74
4	15	20.41	964	0.78

NOTE. — The biweight location of the the disk central surface brightness, central stellar mass surface density, and the degree of maximality of disks are given for each quartile of the sample.

This is comparable to the highest surface brightness disks that exist (Marshall 2004). In the lowest surface density quartile, the typical fraction of maximum disk drops to $\Gamma_* = 0.25$. This confirms and quantifies the well-known result that low surface brightness disks are sub-maximal (de Blok & McGaugh 1997). There is no empirical indication that we have reached a lower limit in Γ_* . Disks lower in surface brightness than the most extreme considered here do exist, though they have yet to be observed with sufficient accuracy to be included here.

The meaning of Γ_* for high surface brightness galaxies is subject to the caveats discussed in §3.1. In particular, the effective definition of maximum disk typically accounts for 84% rather than 100% of the velocity at the peak of the disk contribution (Sackett 1997). If the disks in the highest quartile have 78% of this mass, then they contribute 74% of the velocity at 2.2 scale lengths ($\mathcal{M} \propto V^2$). This is not very different from the sub-maximal contribution of 63% advocated by Bottema (1993) and is certainly within the galaxy-to-galaxy scatter. Kregel, van der Kruit & Freeman (2005) find a slightly lower mean velocity contribution, but their sample is dominated by intermediate surface brightness galaxies, so such a result is consistent with the trend apparent in Fig. 7.

The results in the literature seem broadly consistent,

bearing in mind that a good deal depends on what is really meant by “maximum disk.” The most important point here is that the degree of maximality of a disk depends systematically upon its surface density. There is no magic value of Γ_* that is a fixed fraction for all disks (Bottema 1997; de Blok & McGaugh 1996).

5. CONCLUSIONS

I have explored the Baryonic Tully-Fisher relation for many choices of stellar mass-to-light ratios using a sample of high quality data spanning a large dynamic range in mass. I provide fits to the BTF for each Υ_* . There is a particular choice, based on the minimization of the scatter in the local mass-discrepancy—acceleration relation (the MDAcc; McGaugh 2004), that also minimizes the scatter in the BTF. This optimal BTF is

$$\mathcal{M}_d = 50V_f^4$$

with V_f in km s^{-1} and the total baryonic mass of a galaxy in \mathcal{M}_\odot . This provides a remarkably precise method of estimating the mass of rotating galaxies by observation of a single global observable, the level at which the rotation curve becomes flat.

The form in which the baryonic mass resides, stars or gas, makes no difference to the BTF. Only the sum matters. This strongly suggests that the BTF is a fundamental relation between rotation velocity and baryonic mass. It further implies that there is no other large reservoir of baryons which matter to the sum: the stars and gas observed in spiral galaxies account for essentially all of the baryonic mass therein.

The mass-to-light ratios determined for the optimal BTF are in exceptionally good agreement with stellar population synthesis models. This consistency, together with the agreement between local and global empirical relations connecting baryonic mass to the observed dynamics, implies that the baryonic mass is well determined. This would appear to solve the long standing problem of the uncertainty in the mass of stellar disks.

Using these robust stellar mass estimates, I have examined a variety of evolutionary measures. The stellar fraction, mass-to-light ratio, and color all correlate with each other as one would expect. Little evolved galaxies

with low f_* tend to have blue colors and low Υ_* ; more evolved galaxies have higher stellar fractions, redder colors, and higher mass-to-light ratios. These quantities are also correlated with disk mass and rotation velocity: more massive disks tend to be more evolved.

The degree to which disks are maximal varies systematically with stellar surface density. High surface brightness galaxies tend to be more nearly maximal, typically with $\Upsilon_* \sim 78\%$ of the maximum disk value at $\mu_0^B = 20.4$ mag. arcsec $^{-2}$. Low surface brightness galaxies are sub-maximal, with $\Upsilon_* \sim 25\%$ of maximum disk at $\mu_0^B = 23.3$ mag. arcsec $^{-2}$. There is considerable variation from galaxy to galaxy. In no case is the stellar mass

completely negligible at small radii, a fact that is important to mass models and constraints on the inner slope of the halo mass distribution (core or cusp).

The work of SSM is supported in part by NSF grant AST0206078 and NASA grant NAG513108. SSM is grateful for conversations on this subject with many people, especially Greg Bothun, Bob Sanders, Brent Tully, and Rob Swaters. SSM thanks the Astronomy department of Case Western Reserve University for its hospitality during a sabbatical visit when much of this work was done.

REFERENCES

- Barnes, E.I., Sellwood, J.A., & Kosowsky, A. 2004, *AJ*, 128, 2724
 Begeman, K. G., Broeils, A. H., & Sanders, R. H. 1991, *MNRAS*, 249, 523
 Begum, A., & Chengalur, J.N. 2003, *A&A*, 409, 879
 Begum, A., & Chengalur, J.N. 2004a, *A&A*, 424, 509
 Begum, A., & Chengalur, J.N. 2004b, *A&A*, 413, 525
 Begum, A., Chengalur, J.N., & Hopp, U. 2003, *New Astronomy*, 8, 267
 Begum, A., Chengalur, J.N., & Karachentsev, I.D. 2005, *A&A*, 433, L1
 Bell, E. F. & de Jong, R. S. 2001, *ApJ*, 550, 212
 Bell, E. F., McIntosh, D. H., Katz, N., & Weinberg, M. D. 2003, *ApJS*, 149, 289
 Bothun, G.D., Aaronson, M., Schommer, B., Mould, J., Huchra, J.; Sullivan, W.T., III 1985, *ApJS*, 57, 423
 Bottema, R. 1993, *A&A*, 275, 16
 Bottema, R. 1997, *A&A*, 328, 517
 Broeils, A. H. 1992, Ph.D. thesis, University of Groningen
 Courteau, S., MacArthur, L.A., Dekel, A., van den Bosch, F., McIntosh, D.H., & Dale, D. 2003, *astro-ph/0310440*
 Courteau, S. & Rix, H.-W. 1999, *ApJ*, 513, 561
 de Blok, W.J.G., & McGaugh, S.S. 1996, *ApJ*, 469, L89
 de Blok, W.J.G., & McGaugh, S.S. 1997, *MNRAS*, 290, 533
 de Blok, W.J.G., & McGaugh, S.S. 1998, *ApJ*, 508, 132
 de Blok, W.J.G., McGaugh, S.S., & Rubin, V.C. 2001, *AJ*, 122, 2396
 Eder, J., & Schombert, J. M. 2000, *ApJS*, 131, 47
 Eisenstein, D. J. & Loeb, A. 1996, *ApJ*, 459, 432
 Freeman, K.C. 1999, in *The Low Surface Brightness Universe*, IAU Col. 171, ASP Conference Series 170, 3
 Fuchs, B. 2003, *Ap&SS*, 284, 719
 Gurovich, S., McGaugh, S.S., Freeman, K.C., Jerjen, H., Staveley-Smith, L., & de Blok, W.J.G. 2004, *PASA*, 21, 412
 Hoffman, G. L., Salpeter, E. E., Farhat, B., Roos, T., Williams, H., & Helou, G. 1996, *ApJS*, 105, 269
 Jackson, D.C., Skillman, E.D., Cannon, J.M., & Cote, S. 2004, *AJ*, 128, 1219
 Juneau, S., et al. 2005, *ApJ*, 619, L135
 Karachentsev, I. D., et al. 2003, *A&A*, 398, 479
 Kregel, M., van der Kruit, P.C., & Freeman, K.C. 2005, *MNRAS*, in press (*astro-ph/0501503*)
 Kroupa, P. & Weidner, C. 2003, *ApJ*, 598, 1076
 Marshall, J. 2004, Ph.D. thesis, University of Maryland
 Matthews, L.D., van Driel, W., & Gallagher, J.S. 1998, *AJ*, 116, 1169
 McGaugh, S.S. 2004, *ApJ*, 609, 652
 McGaugh, S.S., & de Blok, W.J.G. 1998a, *ApJ*, 499, 41
 McGaugh, S.S., & de Blok, W.J.G. 1998b, *ApJ*, 499, 66
 McGaugh, S.S., Rubin, V.C., & de Blok, W.J.G. 2001, *AJ*, 122, 2381
 McGaugh, S. S., Schombert, J. M., Bothun, G. D., & de Blok, W. J. G. 2000, *ApJ*, 533, L99
 Milgrom, M. 1983, *ApJ*, 270, 371
 Milgrom, M. & Braun, E. 1988, *ApJ*, 334, 130
 Mo, H. J., & Mao, S. 2004, *MNRAS*, 353, 829
 Meurer, G. R., Mackie, G., & Carignan, C. 1994, *AJ*, 107, 2021
 Navarro, J. F. & Steinmetz, M. 2000a, *ApJ*, 528, 607
 Navarro, J. F. & Steinmetz, M. 2000b, *ApJ*, 538, 477
 Palunas, P. & Williams, T. B. 2000, *AJ*, 120, 2884
 Persic, M., & Salucci, P. 1988, *MNRAS*, 234, 131
 Pfenniger, D., & Revaz, Y. 2005, *A&A*, in press (*astro-ph/0409621*)
 Pierce, M. J., & Tully, R. B. 1988, *ApJ*, 330, 579
 Pizagno, J., Blanton, M.R., Weinberg, D.H., Bahcall, N.A., & Brinkmann, J. 2004, *astro-ph/0410672*
 Portinari, L., Sommer-Larsen, J., & Tantaló, R. 2004, *MNRAS*, 347, 691
 Sackett, P.D. 1997, *ApJ*, 483, 103
 Sakai, S., et al. 2000, *ApJ*, 529, 698
 Sancisi, R. 2003, *IAU Symposium* 220, 192
 Sanders, R. H. 1996, *ApJ*, 473, 117
 Sanders, R.H., & McGaugh, S.S. 2002, *ARA&A*, 40, 263
 Sanders, R. H. & Verheijen, M. A. W. 1998, *ApJ*, 503, 97
 Schombert, J.M., McGaugh, S.S., & Eder, J. 2001, *AJ*, 121, 2420
 Sellwood, J. A. 1999, *ASP Conf. Ser.* 182: *Galaxy Dynamics - A Rutgers Symposium*, 351
 Sprayberry, D., Bernstein, G. M., Impey, C. D., & Bothun, G. D. 1995, *ApJ*, 438, 72
 Steinmetz, M., & Navarro, J.F. 1999, *ApJ*, 513, 555
 Swaters, R.A., Madore, B.F., & Trewhella, M. 2000, *ApJ*, 2000, *ApJ*, 531, L107
 Treu, T., Ellis, R. S., Liao, T. X., & van Dokkum, P. G. 2005, *ApJ*, 622, L5
 Tully, R. B. & Fisher, J. R. 1977, *A&A*, 54, 661
 Tully, R. B. & Verheijen, M. A. W. 1997, *ApJ*, 484, 145
 van Albada, T. S. & Sancisi, R. 1986, *Royal Society of London Philosophical Transactions Series A*, 320, 447
 van den Bosch, F. C. 2000, *ApJ*, 530, 177
 Verheijen, M. A. W. 1997, Ph.D. thesis, University of Groningen
 Verheijen, M. A. W. 2001, *ApJ*, 563, 694
 Verheijen, M. A. W. & Sancisi, R. 2001, *A&A*, 370, 765
 Warren, B.E., Jerjen, H., & Koribalski, B.S. 2004, *AJ*, 128, 1152
 Zavala, J., Avila-Reese, V., Hernández-Toledo, H., & Firmani, C. 2003, *A&A*, 412, 633
 Zwaan, M.A., van der Hulst, J.M., de Blok, W.J.G., & McGaugh, S.S. 1995, *MNRAS*, 273, L35